



Contents lists available at ScienceDirect

Arabian Journal of Chemistry

journal homepage: www.ksu.edu.sa

Original article

Carbon dots-doped melamine–formaldehyde microsphere as a dual functional material for sensing and adsorption of oxytetracycline

Lu-Shuang Li ^{a,1}, Su Li ^{a,1}, Zong-Mei Huang ^a, Yan-Ting Song ^a, Wei Gong ^b, Jing Li ^{b,*}^a Key Laboratory of Tropical Biological Resources of Ministry of Education, School of Pharmaceutical Sciences, Collaborative Innovation Center of One Health, Hainan University, Haikou 570228, China^b Xiangyang Central Hospital, Affiliated Hospital of Hubei University of Arts and Science, Xiangyang 441021, China

ARTICLE INFO

Keywords:

Carbon dots
Melamine-formaldehyde
Fluorescence sensor
Adsorption
Oxytetracycline

ABSTRACT

The abuse of oxytetracycline (OTC) leaves serious environmental residues and triggers accumulation in organisms, constituting a threat to human health. Constructing an effective platform based on dual-functional materials for monitoring and removing OTC residues is a preferable solution. Herein, we proposed a novel composite material by doping carbon dots (CDs) into melamine–formaldehyde microsphere (MFM) through a one-pot method and named CDs@MFM, which inherited the fluorescence property of CDs and porous structure of MFM simultaneously. CDs@MFM demonstrated dual functions for the detection and removal of OTC concurrently within a few minutes, with its performance compared in detail with bare CDs and MFM as controls. By virtue of the pre-enrichment effect attributed to its porous structure, CDs@MFM exhibited a lower detection limit for OTC than bare CDs (0.027 mg/L vs 0.067 mg/L) and a higher adsorption capacity than MFM (73.01 mg/g vs 68.76 mg/g) resulting from more affiliated functional groups available for OTC provided by the CDs. Overall, CDs@MFM has proven to be an efficient and convenient candidate capable of monitoring and removing OTC synchronously, and this work offers an avenue for the design of dual-functional materials in the field of environmental science.

1. Introduction

As a member of the tetracycline antibiotics (TCs), oxytetracycline (OTC) has been widely applied in the breeding industry to prevent and treat bacterial infectious diseases or promote the growth of livestock due to its desirable antibacterial effects, good oral absorption and low cost (Wang et al., 2018, Fu et al., 2021). However, the abuse of OTC may leave residual presence in environment media and animal-derived foods, such as milk, meat and eggs (Chen et al., 2020). Excessive or long-term exposure to OTC may cause physical discomfort, skeletal deformity, or growth inhibition (Wang et al., 2020), which constitute a serious threat to human health. In addition, the excessive residues of OTC in the environment can also increase antibiotic resistance in bacteria, thus exacerbating a global problem (Lu et al., 2023). Therefore, an effective platform for monitoring and removing OTC residues is greatly needed. Fluorescence analysis method has attracted much attention due to the advantages of simple operation, low cost, high sensitivity and selectivity in the detection of OTC (Wang et al., 2018). As for disposing OTC

residue, adsorption technology has occupied a prominent place for the low cost, high efficiency, easy operation and eco-friendliness (Yang et al., 2020, Qi et al., 2023).

In recent researches on pollution monitoring and disposing, scientists fabricated complexes by combining porous materials with luminophores to integrate fluorescence detection and adsorption functions together (Qin et al., 2021, Hu et al., 2022). In this way, complicated operations were avoided and costs were reduced. So far, only a few dual-functional advanced materials for simultaneously sensing and adsorption of TCs have been reported. These researches typically achieved bifunctionality by integrating Eu and metal–organic frameworks through a variety of methods (Li et al., 2021, Zhao et al., 2021, Wu et al., 2022, Li et al., 2023), while they also displayed disadvantages of environment unfriendliness, complex preparation and modification processes, and high costs. Therefore, the development of novel dual-functional materials remains an ongoing challenge.

Carbon dots (CDs) are emerging nanomaterials with excellent optical properties which can be used in the construction of fluorescence sensors

* Corresponding author.

E-mail address: Lijing@hbuas.edu.cn (J. Li).¹ Lu-Shuang Li and Su Li contributed this work equally.<https://doi.org/10.1016/j.arabjc.2024.105972>

Received 29 April 2024; Accepted 17 August 2024

Available online 18 August 2024

1878-5352/© 2024 The Author(s). Published by Elsevier B.V. on behalf of King Saud University. This is an open access article under the CC BY-NC-ND license (<http://creativecommons.org/licenses/by-nc-nd/4.0/>).

(Li et al., 2018, Li et al., 2023). The advantages of CDs over traditional luminophores (quantum dots, rare earth elements, organic dyes, etc.) include their low cost, high stability, and little toxicity. At present, there have been some reports on the construction of OTC fluorescence sensors with CDs (Guo et al., 2023, Wang et al., 2023, Li et al., 2024). Red-emitting carbon dots (R-CDs) were prepared with urea and resazurin and exhibited a remarkable fluorescence reduction towards TCs, thus enabling the trace detection of TCs (Wang et al., 2023). Guo et al. synthesized the dual-excitation carbon dots using microwave radiation to construct a ratiometric sensor for doxycycline (DOX), and achieved a low detection limit of 61 nM (Guo et al., 2023). Melamine-formaldehyde resin microsphere (MFM) is a porous material with simple preparation methods, low price, pronounced thermal and solvent stability, indicating high potential as an adsorption substrate for contaminants in water environment, such as heavy metal ions and other organic pollutants (Liu et al., 2015, Ming et al., 2016). We also applied MFM for the removal of perfluorooctanoic acid from water successfully in the previous work and it revealed satisfactory pH and temperature resistance (Li et al., 2017).

In this study, a novel advanced composite material for detection and removal of OTC was proposed initially with CDs as the fluorescent sensing unit and MFM as the adsorption substrate. The dual-functional material was synthesized through a one-pot process and named CDs@MFM. Comparative experiments were conducted to inspect its applicability in the detection and removal of OTC. Possibly due to the pre-enrichment effect, the sensor constructed with CDs@MFM had a wider linear range and a lower LOD than bare CDs. Moreover, benefiting from the affinity of CDs to OTC, CDs@MFM exhibited superior adsorption performance of OTC with higher kinetic constant and adsorption capacity than MFM. In comparison to other CDs-based sensors for tetracyclines, the proposed material demonstrates dual functionality with favorable detection sensitivity and acceptable adsorption capacity. Furthermore, the adoption of CDs as the fluorescent signal sensing element herein offers the advantages of easy availability, cost-effectiveness, and environmental friendliness. In summary, this work not only provided a powerful strategy to monitor and dispose OTC in contaminated aqueous solution simultaneously, but also opened an exciting way for the design and preparation of dual-functional materials.

2. Material and methods

2.1. Chemicals and reagents

Citric acid and melamine were purchased from Shanghai Aladdin Biochemical Technology Co., Ltd. (Shanghai, China). Formaldehyde solution (37 wt%), methanol, ethanol, HCl and NaOH were obtained from Xilong Science Co., Ltd (Shantou, China). Chlorotetracycline (CTC), oxytetracycline (OTC), tetracycline (TET), serine (Ser), glycine (Gly), cysteine (Cys), valine (Val), tryptophan (Try), leucine (Leu), lysine (Lys), streptomycin (SM), ampicillin (AMP), chloramphenicol (CAP) and EDTA were supplied by Shanghai Macklin Biochemical Co., Ltd (Shanghai, China). Ultrapure water was obtained from a Milli-Q water purification system (Millipore, Bedford, MA, USA).

2.2. Instrument and Characterization

Scanning electron microscope (SEM) and transmission electron microscopic (TEM) images were captured by a JSM-35CF microscope (JEOL, Japan) and a JEM-2100 microscope (JEOL, Japan), respectively. Fourier transform infrared spectroscopic (FTIR) spectra were recorded by an AVATAR 360 spectrometer (Thermo, USA). X-ray photoelectron spectroscopy (XPS) measurement was carried out on an ESCALAB 250Xi electron spectrometer (Thermo, USA). The nitrogen adsorption-desorption isotherms were obtained through a TriStar II surface area analyzer (Micromeritics, USA). UV-vis and fluorescence spectra were recorded by an UV-2600 and a F-4700 spectrophotometer (Hitachi,

Japan), respectively. The quantum yield (QY) was determined at excitation wavelength of 360 nm with quinine sulfate as a reference, of which QY was 54 % in 0.01 M H₂SO₄ solution.

2.3. Preparation of CDs, MFM and CDs@MFM

For CDs, the synthesis method followed the previous work with some modification (Li et al., 2018). 2.0 g of citric acid and 30 mg of melamine were dissolved in 10 mL of ultrapure water. After adding 0.6 mL of formaldehyde solution, the obtained mixture was transferred into a Teflon-lined autoclave and reacted at 180 °C for 10 h. After cooling down to room temperature, the deep yellow solution was filtered through a 0.22 μm membrane and dialyzed against ultrapure water through a dialysis bag (MWCO 1000) for 24 h. The solvent from the purified CDs solution was removed by the rotary vapor.

For CDs@MFM, melamine (1.2 g), formaldehyde solution (10 mL) and ultrapure water (20 mL) were firstly mixed and stirred at 70 °C till the solution became clear and transparent, thus obtaining the prepolymer solution. Then, 5.0 mL of CDs solution with different concentrations were mixed with the isometric prepolymer solution and heated for 8 h at 160 °C into a Teflon-lined autoclave. Thereafter, the formed solid was collected by centrifugation, washed with ethanol and ultrapure water, and dried at 80 °C successively, thus obtained CDs@MFM. The MFM were prepared using the same procedure except without adding CDs.

2.4. Fluorescent sensing of OTC

In the comparative study, fluorescent sensing experiments were conducted with both bare CDs and CDs@MFM. OTC stock solution was prepared in methanol and stored at 4 °C. OTC standard working solution series at different concentrations were prepared by diluting the stock solution in ultrapure water. CDs@MFM powders were dispersed into ultrapure water with sonication and diluted to obtain a CDs@MFM stock solution (40 mg mL⁻¹) and the dispersion was remixed by vortex prior to use.

For detection of OTC, 200 μL of CDs or CDs@MFM solution was added to 5.0 mL of sample solution in a centrifuge tube. After mixing thoroughly and incubating for 5 min, the solution was subjected to fluorescence measurement at the excitation wavelength (E_x) of 340 nm and emission wavelength (E_m) of 450 nm, respectively. The quenching efficiency was evaluated with F/F₀ as the criterion, in which F and F₀ represented severally the fluorescence intensity of the CDs/CDs@MFM solution with and without OTC. The limit of detection (LOD) was calculated as 3δ/k, where δ is the standard deviation of the fluorescent intensity of CDs/CDs@MFM, k is the gradient of the linear relationship between the fluorescent intensity of CDs and the concentration of OTC. To assess the selectivity of the proposed sensor, the influence of other ions (10 mg/L) and small molecules (10 mg/L) on the fluorescent intensity of CDs@MFM was investigated under the same conditions. For interference experiments, the sensing was evaluated by measuring the fluorescence response of CDs@MFM to OTC (10 mg/L) in the presence of each analyte (10 mg/L).

The sensor was applied for OTC detection in lake water to verify the reliability. The collected lake water samples were filtered through a membrane, and the filtrate was used for subsequent testing. The spiked samples with different concentrations of OTC were applied for recovery experiments. The recovery was calculated through Eq. (1),

$$\text{Recovery (\%)} = \frac{C_{\text{measured}}}{(C_{\text{added}} + C_0)} \times 100\% \quad (1)$$

where C_{measured} is the concentration calculated by the fitted regression equation, C_{added} is the spiked concentration and C₀ represents the actual concentration of OTC in lake water.

2.5. OTC adsorption experiments

For comparison, the adsorption performance of both CDs@MFM and MFM were studied simultaneously. A typical adsorption experiment was performed as follows: 200 μL homogeneous CDs@MFM or MFM stock solution was added to 5 mL of the OTC solution. Adsorption was performed on a temperature-controlled rotary shaker kept out of exposure to light. After a fixed duration, the suspension was filtered, and the concentration of residual OTC was determined and calculated through the absorbance of the supernatant at 372 nm. The adsorption capacity of the adsorbents toward OTC was calculated according to the Eq. (2),

$$q_t = \frac{(C_0 - C_t) \times V}{m} \quad (2)$$

where C_0 (mg/L) is the initial concentration of OTC, C_t (mg/L) is the concentration of OTC in the supernatant at an interval, V (L) is the volume of the adsorption system, m (g) is the mass of the adsorbent. The impacts of initial pH value on the adsorption performance of CDs@MFM/MFM were investigated by adjusting the pH value of the OTC solution with HCl and NaOH.

Kinetic adsorption tests were carried out at the initial OTC concentration of 50 mg/L. The pseudo-first order (Eq. (3)) and the pseudo-second-order (Eq. (4)) kinetic models were adopted to simulate the adsorption process as follows:

$$\ln(q_e - q_t) = \ln q_e - k_1 t \quad (3)$$

$$\frac{t}{q_t} = \frac{1}{k_2 q_e^2} + \frac{t}{q_e} \quad (4)$$

where q_t and q_e are the adsorption capacity at time “ t ” and equilibrium (mg/g); k_1 , and k_2 represents the rate constants of the pseudo-first order and the pseudo-second-order kinetic models, respectively (Gai et al., 2020, Zhang et al., 2021, Hu et al., 2022).

For the investigation of adsorption thermodynamics, the adsorption was conducted at different initial concentrations of OTC solution (5 ~ 200 mg/L) at specific temperature (303 K, 313 K, 323 K). The experimental data were then fitted to Langmuir (Eq. (5)) and Freundlich (Eq. (6)) isotherm models by nonlinear regression (Gai et al., 2020, Li and Xu, 2020, Zhang et al., 2021). Corresponding equations are listed as below:

$$\frac{C_e}{q_e} = \frac{1}{q_{max} k_L} + \frac{C_e}{q_{max}} \quad (5)$$

$$q_e = k_F C_e^{1/n} \quad (6)$$

where q_e and q_{max} are the adsorption capacity at equilibrium and the theoretical maximum amount of adsorption (mg/g). C_e is the residual OTC concentration at equilibrium; k_L and k_F represent the constants of

Langmuir and Freundlich isotherm models, respectively. n refers to heterogeneity factor.

3. Results and discussion

3.1. Characterization of CDs and CDs@MFM

As the fluorophores deployed for sensing, CDs were synthesized through the hydrothermal method. The morphology and size of the CDs were characterized with TEM. As shown in Fig. 1A, CDs were quasi-spherical nanoparticles and could evenly disperse in aqueous solution. The average diameter was calculated to be 3.3 ± 0.7 nm through a Nano Measurer 1.2 software (inset of Fig. 1A). The XPS survey (Fig. 1B, blue line) indicated that the CDs were predominantly composed of C, O and N elements, with a calculated composition of 71.69 %, 13.36 % and 14.96 %, respectively. The high-resolution C 1 s spectrum of CDs (Fig. 1C) exhibited three peaks at 284.84 eV, 286.24 eV, and 289.02 eV, corresponding to C–C, C–S/C–N/C–O, and C=N/C=O bonds, respectively. The N 1 s spectrum of CDs (Fig. 1D) displayed two subpeaks at 399.88 eV (N–C) and 401.74 eV (N–H), while the O 1 s spectrum (Fig. 1E) showed two peaks at 532.15 eV (C=O) and 533.41 eV (C–OH/C–O–C). FTIR analysis of CDs was also conducted. The broad absorption band at 3436 cm^{-1} in Fig. 1F (blue line) was attributed to O–H/N–H stretching vibrations. Furthermore, absorption peaks at 2978 cm^{-1} , 1722 cm^{-1} , 1639 cm^{-1} , and 1224 cm^{-1} were associated with C–H, C=O, C=C, and C–O/C–N stretching vibrations, respectively. According to these results, there were multiple functional groups on the surface of CDs, ensuring their water solubility and providing vast chemical interaction sites (Bishwal et al., 2023).

The optical properties of the CDs were investigated through UV–vis absorption and fluorescence spectra (Fig. 1G). The UV absorption spectrum is associated with specific electronic transitions within molecules. In the UV–vis spectrum of CDs (green line), absorption is observed in the 200 nm to 400 nm range, which is attributed to the presence of both $\pi-\pi^*$ and $n-\pi^*$ transitions (Alimohammadi et al., 2023). A slight shoulder at 290 nm is noted, possibly originating from the $n-\pi^*$ transition of the C=O/C=N bonds, indicating a notable presence of C=O/C=N on CDs. In addition, with the increase in excitation wavelength from 310 nm to 370 nm, the maximum emission wavelength of CDs is redshifted, demonstrating that the excitation-dependent photoluminescence behavior (Venugopalan and Vidya, 2023, Hu et al., 2024). It is a typical property of CDs, which was attributed to the various surface fluorescent emitting groups or heterogeneous particle sizes. The maximum fluorescence intensity of CDs was achieved at the E_x of 340 nm and E_m of 430 nm, which were further applied for the photometry measurement in the subsequent experiments. The QY of CDs was calculated to be 39.5 %, which was relatively higher than many other works (Fu et al., 2021, Li et al., 2023, Li et al., 2024, Qi et al., 2023,

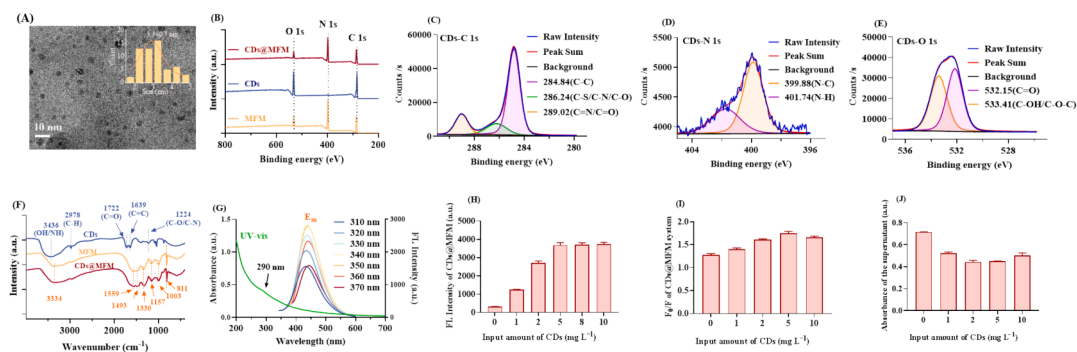


Fig. 1. Characterization of the materials. (A) TEM image of CDs (inset: size distribution diagram of CDs). (B) XPS full-scan survey of CDs, MFM and CDs@MFM. (C–E) High-resolution XPS spectra of CDs. (F) FTIR spectrum of CDs, MFM and CDs@MFM. (G) UV–vis absorption curve and fluorescence emission spectra of CDs under E_x of 310 ~ 370 nm. (H–J) Optimization of the input amount of CDs in the preparation system of CDs@MFM in terms of fluorescence intensity, quenching efficiency and adsorption capacity.

Rasheed, 2023), exhibiting their excellent potential for following sensor procedure.

CDs@MFM were prepared by the one pot method. To simultaneously improve the fluorescence intensity, sensing performance, and adsorption capacity of CDs@MFM, the amount of CDs added into the preparation system was optimized, respectively. As presented in Fig. 1H, with the rising input of CDs, the fluorescence intensity of obtained CDs@MFM increased rapidly at first and remained constant subsequently indicating the doping amount of CDs had gradually reached saturation. The quenching efficiency of CDs@MFM fluorescence by OTC first increased, then decreased, before reaching the peak at the input amount of 5 mg L^{-1} (Fig. 1I). Similarly, the adsorption capacity of OTC by CDs@MFM also increased first and then decreased as doping amount of the CDs increased (Fig. 1J). According to the above results, the increase of CDs doping amount was not always beneficial to the detection and adsorption performance but would play a negative role after reaching the optimal level. This may be explained by that excessive CDs may block the pores of the material to some extent, and affected the interactions between CDs@MFM and OTC during the sensing and adsorption process.

The morphology and porosity of CDs@MFM were characterized by SEM, HRTEM and specific surface area analysis, with MFM as a comparison. As shown in Fig. 2A~2B, both the prepared CDs@MFM and MFM exhibited good dispersion and showed no obvious distinct in the magnification of SEM. The HRTEM images clearly identified the mesoporous structure of MFM and CDs@MFM (insets in Fig. 2A~2B). Compared with MFM, the uniform distribution of CDs in CDs@MFM was also observed. The nitrogen adsorption-desorption isotherms of the two materials were depicted in Fig. 2C~2D. The specific surface area of MFM and CDs@MFM were calculated to be $86.6 \text{ m}^2/\text{g}$ and $96.1 \text{ m}^2/\text{g}$, respectively, based on the Brunauer-Emmett-Teller equation. Using the Barrett-Joyner-Halenda method, the average pore diameter and pore volume of MFM were 7.4 nm and $0.18 \text{ cm}^3 \text{ g}^{-1}$, respectively, and those of CDs@MFM were 6.2 nm and $0.12 \text{ cm}^3 \text{ g}^{-1}$. It could be seen that CDs@MFM had a slightly reduced pore diameter and pore volume, but a little larger surface area. It was speculated that the doping of nanoscale CDs may occupy a certain amount of interstitial space and increase the roughness of the material surface or form interspaces between

nanoparticles (Li and Xu, 2020). In any case, the porosity of CDs@MFM was sufficient to guarantee the potential for subsequent detection and adsorption applications.

The chemical compositions of CDs@MFM were characterized through FTIR and XPS spectroscopy. As shown in Fig. 1B, the XPS survey spectra indicated the presence of C 1s, O 1s and N 1s in all of the three materials, illustrating their identical elemental composition but differing in several proportion. The respective high resolution XPS spectra of MFM and CDs@MFM were depicted in Fig. 3A~3F. As calculated, MFM composed of 43.25 % C, 48.25 % N and 8.5 % O. The proportions of C, N and O in CDs@MFM were 48.59 %, 46.34 % and 9.06 %, respectively. According to these specific data, there were less N, and more C and O in CDs@MFM than MFM. These results demonstrated the successful doping of CDs, which moderated the elemental composition of MFM. As depicted in the FTIR spectra (Fig. 1F), CDs@MFM (red line) was mostly similar to MFM (yellow line), with only a slight shift in peak positions. The absorption peaks at 3334 cm^{-1} (O-H/N-H), 1559 cm^{-1} , 811 cm^{-1} (1,3,5-triazine ring), 1493 cm^{-1} ($-\text{CH}_2$), 1330 cm^{-1} (C-H), 1157 cm^{-1} (C-N) and 1003 cm^{-1} (C-O) were all typical characters of MFM (Li et al., 2017), indicating the structure reservation of MFM in CDs@MFM. In comparison with bare CDs (blue line), the peaks at 1722 cm^{-1} (C=O) and 1639 cm^{-1} (C=C) were absent, which may be due to relatively small quantity of CDs doped into MFM. The weak signals of CDs were covered for the introduce of bulk-structural MFM. It can also be confirmed by the higher similarities found in FIIR spectra between MFM and CDs@MFM. Furthermore, the peaks at 3436 cm^{-1} (O-H/N-H) and 1224 cm^{-1} (C-O/C-N) exhibited blue shifted to 3334 cm^{-1} and 1157 cm^{-1} , respectively, which may be indicative of the formation of hydrogen bonds between CDs and MFM (Qin et al., 2021). As shown in Fig. 3G, the fluorescence spectra of CDs@MFM were almost identical to those of CDs (Fig. 1G), demonstrating that immobilized CDs remained their fluorescence.

The fluorescence stability of CDs and CDs@MFM was studied in terms of pH, ionic strength and illumination. As shown in Fig. 3H, the fluorescence intensity of CDs remained relatively stable in the pH range of 3 to 10. When the pH was more extreme (<3 or >10), CDs@MFM exhibited higher stability than CDs, which may be due to the immobilization of CDs that limits the protonation and deprotonation of the

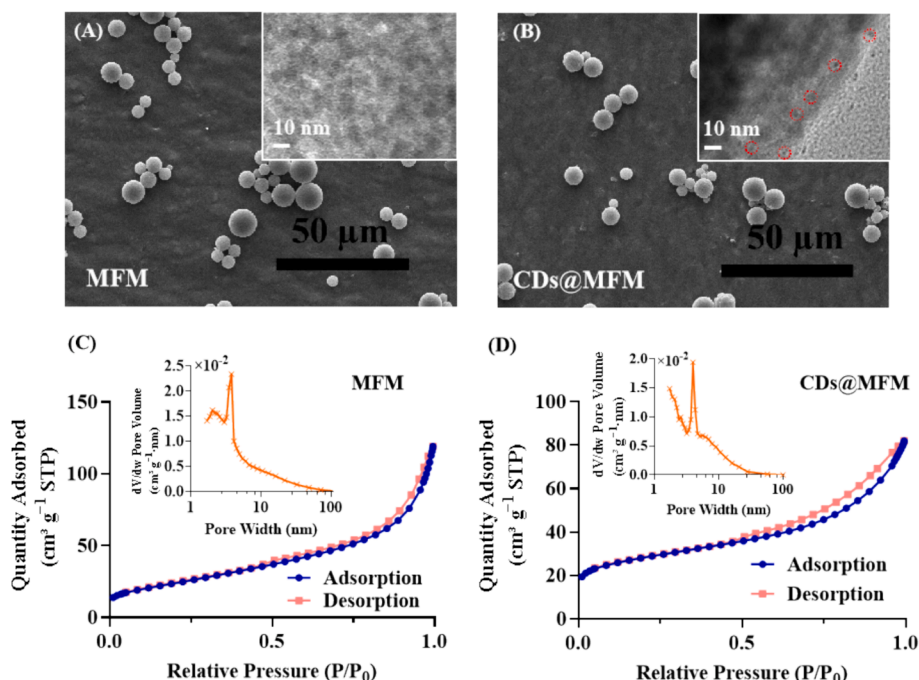


Fig. 2. Characterization of the materials. (A~B) SEM images and HRTEM images. (C~D) Nitrogen adsorption-desorption isotherms and pore size distribution.

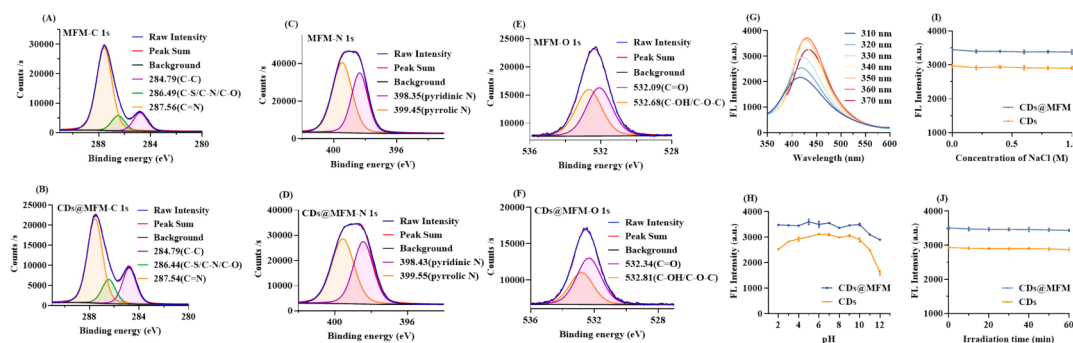


Fig. 3. Characterization of the materials. (A~F) High resolution XPS spectra of MFM and CDs@MFM. (G) Fluorescence emission spectra of CDs@MFM under E_x of 310 ~ 370 nm. (H~J) Stability of CDs and CDs@MFM in terms of pH, ion strength and photobleaching.

surface functional groups of CDs (Wang et al., 2023). The presence of NaCl in high concentration or longtime continuous irradiation at 360 nm had almost no influence on the fluorescence intensity of CDs or CDs@MFM, reflecting their excellent ionic stability and photostability (Fig. 3I~3J).

To sum up, all the characterization results verified that the original structure of MFM was not destroyed during the preparation process and the fluorescence properties of CDs were preserved efficiently. It is practicable to construct a dual-functional system for detecting and removing OTC concurrently based on CDs@MFM.

3.2. Detection of OTC

In the preliminary experiment, we found that the fluorescence of CDs could be effectively quenched by OTC. To investigate the OTC sensing performance, CDs and CDs@MFM were attempted simultaneously and compared in the following sensing experiments. Firstly, the sensing conditions including pH and incubation time were optimized. As shown in Fig. 4A, with pH in the range between 2 and 9, the fluorescence of both CDs and CDs@MFM showed obvious response to OTC but with no significant variation. However, with further increase of pH, the quenching effect of OTC on their fluorescence was significantly

weakened. In addition, both the fluorescence of CDs and CDs@MFM showed a quick response to OTC within 5 min and would stay relatively constant thereafter (Fig. 4B). For simple operation and rapid detection, a sample pH of 7 and incubation time of 5 min were adopted in the subsequent experiments.

To explore the responding mechanism, fluorescence spectra, UV-vis absorption spectra and fluorescence decay curves were analyzed and depicted in Fig. 4C~4D (Rasheed, 2023, Zu et al., 2017). As shown in Fig. 4C, after adding OTC to the sensing system of CDs, the absorption spectrum of the system (purple line) displayed a simple overlay of the spectra of CDs (orange line) and OTC (green line), indicating no changes in chemical structures, suggesting the absence of a static quenching mechanism (Li et al., 2023). As depicted, the UV-vis absorption spectrum of OTC (green line) significantly overlaps with the fluorescence excitation spectrum of CDs (yellow line) and slightly overlaps with the fluorescence emission spectrum of CDs (blue line). This suggests that the quenching process may involve the inner filter effect (IFE) rather than fluorescence resonance energy transfer (FRET) (Zu et al., 2017). The fluorescence decay curves of CDs before and after OTC addition were measured. As shown in Fig. 4D, the decay curves were well fitted with a double exponential decay function, and the average fluorescent lifetime were calculated to be 5.12 ns and 3.77 ns, respectively. This variation in

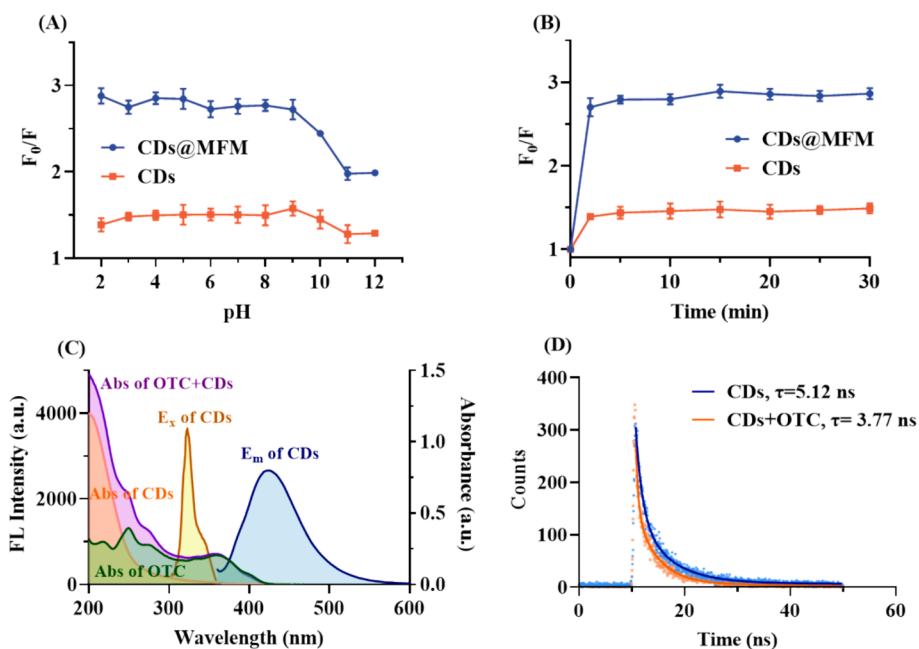


Fig. 4. Optimization of the sensing conditions and mechanism exploration of CDs to OTC. (A) Influence of pH on the quenching efficiency (F_0/F). (B) Variation of F_0/F versus the incubation time. (C) UV-vis absorption curves of the CDs before and after adding OTC and fluorescence spectra of CDs. (D) Time-resolved decay curves of CDs with and without OTC and the fitted lines with the double exponential decay function.

lifetime of CDs in the absence and presence of OTC suggested that dynamic quenching mechanism may be involved (Zu et al., 2017, Liu et al., 2021). In summary, the sensing procedure of CDs to OTC may through a combination of dynamic quenching and IFE mechanisms (Wu et al., 2022, Liu et al., 2022, Liu et al., 2025).

To evaluate the quantification capacity of the proposed sensor, OTC solutions at various concentrations were employed. As illustrated in Fig. 5A~5B, the fluorescence intensity of both CDs and CDs@MFM gradually decreased with the increase concentration of OTC. As observed, at the same concentration of OTC, there was a higher fluorescence quenching effect on the CDs@MFM than CDs. The Stern–Volmer equation (Eq. (7)) was applied to further evaluate the quenching efficiency of the two sensors (El-Malla et al., 2022),

$$\frac{F_0}{F} = 1 + K_{SV}[A] \quad (7)$$

where K_{SV} is the quenching constant, F and F_0 represent the fluorescence intensity of the CDs/CDs@MFM solution with and without OTC, respectively; $[A]$ is the concentration of OTC (mg/L). As shown in Fig. 5C, the quenching efficiency exhibited good linearities with OTC concentration ranges of 0.05 ~ 10 mg/L for CDs@MFM and 0.1 ~ 10 mg/L for CDs, respectively. K_{SV} was calculated to be 0.1057 mg⁻¹ L and 0.0427 mg⁻¹ L. The much larger K_{SV} implied that CDs@MFM has higher sensitivity to OTC than CDs. Furthermore, the limit of detection (LOD) was calculated by $3\sigma/k$, where σ is the standard deviation, and k is the slope of the linear regression curve. The sensor constructed with CDs@MFM had a lower LOD compared with CDs (0.027 mg/L vs 0.067 mg/L). The CDs@MFM demonstrated a lower detection limit for OTC compared to CDs alone, benefiting from the optimal specific surface area and pore structure of the composite. OTC is adsorbed and concentrated on the surface of CDs@MFM, resulting in an increased local concentration around the CDs, a phenomenon known as the preconcentration effect (Zhou et al., 2018; Wu et al., 2022). This preconcentration effect enhances the interaction between OTC and the CDs within the framework, significantly improving the fluorescence quenching efficiency and the overall efficacy of OTC sensing.

In summary, CDs@MFM probe provided wider linear range and lower LOD than CDs for OTC detection, which is more conducive to the monitoring of OTC residues in the environment. Also, compared to the other reported CDs or dual functional materials-based sensors in Table 1, CDs@MFM showed comparable or better detection ability towards OTC.

To evaluate the selectivity and anti-interference of the sensor, the

Table 1

Comparison of CDs@MFM detection and adsorption performance with other fluorescence sensors based on CDs, other adsorbents or dual functional materials.

Material	Drug	Linear range	LOD	q_m (mg/g)	Ref.
R-CDs	OTC	4–50 μM	64.6 nM	/	(Wang et al., 2023)
C-CQDs	OTC	0–100 μM	120 nM	/	(Zhu et al., 2022)
N-CQDs	OTC	0–20 μM and 20–100 μM	265 nM	/	(Wang et al., 2022)
TTS	TC	/	/	15.45	(Sun et al., 2022)
Zoogloea sp. MFQ7	TC	/	/	52.21	(Chang et al., 2021)
SA-Cu beads	TC	/	/	53.26	(Zhang et al., 2019)
CD@AMP/Eu NCPs	OTC	0.2–60 μM	25 nM	/	(Chen et al., 2020)
Eu ³⁺ @BrPz-COF	TC	0.5–150 μM and 150–350 μM	7 nM	205.34	(Liu et al., 2023)
CDs@HZIF-8	OTC	0.5–7 μM and 7–40 μM	29.46 nM	1328.42	(Li et al., 2022)
ROD-Zn1 and ROD-Zn2	TC	0–45 μM and 0–45 μM	110 nM and 120 nM	92.3 and 87.6	(Gai et al., 2020)
CDs@MFM	OTC	0.05–10 mg/L (0.11–21.72 μM)	0.027 mg/L (60 nM)	73.59	This work

impacts of potential interfering substances on CDs@MFM fluorescence were studied. Fig. 5D revealed that among various small molecules, CTC and TET can also notably decrease fluorescence intensity due to the similar structure, which demonstrates the strong selectivity of the sensor towards tetracyclines. The incapability of distinguish different tetracyclines is a common problem of single sensing element, which should not be over criticized. In addition, Fe³⁺ could also quench the fluorescence to some extent. However, given that the typical concentration of Fe³⁺ in

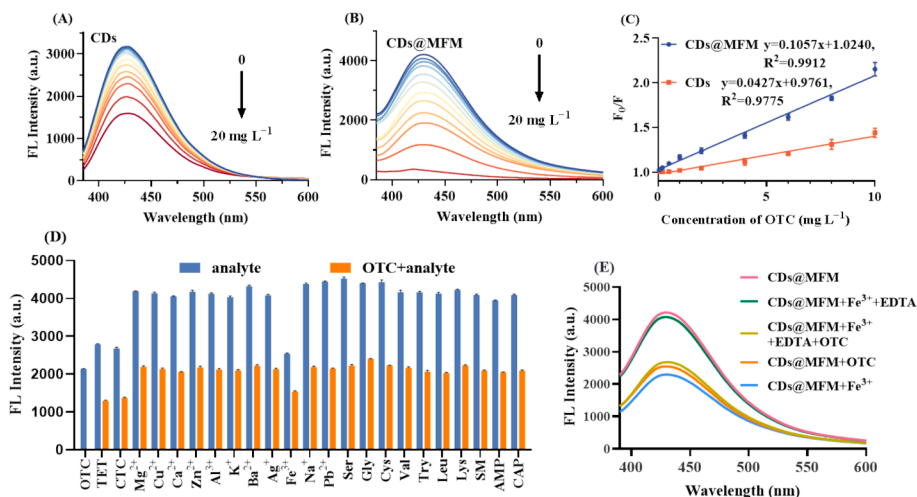


Fig. 5. Fluorescence sensing performance of CDs and CDs@MFM to OTC. (A) Fluorescence spectra of CDs with OTC at various concentrations. (B) Fluorescence spectra of CDs@MFM with OTC at various concentrations. (C) The linear fitting of F_0/F with the concentrations of OTC. (D) The selectivity and anti-interference of CDs@MFM in response to OTC over other ions and small molecules (Concentrations of all the analytes were 10 mg/L). (E) The interference of Fe³⁺ (10 mg/L) on the sensing system and the eliminating effect through adding EDTA.

surface water is approximately 0.1 mg/L, much lower than the experimental concentration of 10 mg/L, interference from Fe^{3+} in real samples could be ignored theoretically. Even if in the Fe^{3+} -enriched environment samples, the interference on the detection may be mitigated through pretreating samples with EDTA (Stacy et al., 2024). The comparison of the fluorescence spectra of CDs with OTC in the absence or presence of Fe^{3+} and EDTA were conducted and depicted in Fig. 5E. The fluorescence of CDs@MFM quenched by Fe^{3+} can be restored by EDTA (pink line vs green line vs blue line). Detection of OTC in samples with high Fe^{3+} content was not affected when it was pretreated with EDTA (yellow line vs orange line). In general, the selectivity and anti-interference of the proposed sensor based on CDs@MFM is acceptable.

The proposed sensor was deployed to determine OTC level in lake water samples, which were collected from Dongpo Lake at Hainan University. The water displayed a light yellowish-brown color, with a measured pH of 8.12 and a salinity of 15.0. The concentrations of various water quality-related chemicals were as follows: ammonia at 1.555 μM , nitrite at 2.820 μM , and reactive phosphate at 1.607 μM . The results showed that no residual OTC was detected in the collected lake water samples. As listed in Table 2, lake water samples spiked with OTC at three concentration levels (6.00 mg/L, 2.00 mg/L, 0.10 mg/L) were tested, and the recoveries ranged from 92.7 % to 115.0 %, with relative standard deviation (RSD) lower than 5.25 %. These results indicated that the proposed sensor was a viable strategy for monitoring OTC in lake water samples.

3.3. Adsorption of OTC

As a dual functional material, in addition to sensing, the adsorption performance of CDs@MFM on OTC was also investigated to verify its potential for environmental remediation, with MFM as the comparative. The pH of solution is a critical parameter which may change the chemical state of adsorption sites and target chemicals, thus affecting the adsorption performance. To ensure high performance of CDs@MFM system for OTC adsorption, the adsorption capability was evaluated at different initial pH values (3.0 ~ 11.0). As presented in Fig. 6A, the adsorption capacity of both CDs@MFM and MFM showed no significant difference in the studied pH range, demonstrating that pH had little effect on the interactions between adsorption site and OTC. It is noteworthy that the adsorption capacity of CDs@MFM for OTC was much greater than that of MFM at any pH, preliminarily proving that doping of CDs was beneficial to improving the adsorption performance. To maintain a simple and consistent approach with the sensing conditions, pH of 7 was selected in the subsequent adsorption experiments.

The time-course adsorption experiments were performed to explore the adsorption kinetics of CDs@MFM and MFM. As observed (scatter plots in Fig. 6B), under the selected experimental conditions, the adsorbed amount of OTC of both CDs@MFM and MFM increased sharply within the first 5 min upon addition of the material and gradually reach equilibrium within 15 min. The rapid adsorption may be attributed to the strong interactions between the adsorbents and OTC and the low mass transfer impedance of the material, which benefited from the

doping of CDs as well as the porous structure of MFM. This rapid adsorption was in agreement with the short time required for fluorescent sensing as described in Section 3.2. To gain insight into the adsorption process, the data were fitted onto pseudo-first order (PFO) and the pseudo-second order (PSO) kinetic models (Fig. 6B). The parameters used to fit the experimental curves to the models were displayed in Table 3. It can be observed that the adsorption process was well fitted to both pseudo-first order and pseudo-second-order models with both correlation coefficients (R^2) higher than 0.98. The calculated theoretical adsorption capacities at equilibrium were very close to the experimental value, which indicated that the physical adsorption and chemical adsorption were both involved in the adsorption process (Li et al., 2017). As calculated, the kinetic constants of CDs@MFM were all larger than MFM, suggesting that the doping of CDs may have provided stronger interaction force between the adsorbent and OTC, thus increasing the adsorption rate.

The adsorption isotherms of MFM at 303 K and CDs@MFM at different temperatures (303 K, 313 K and 323 K) were performed and illustrated in Fig. 6C~6D. For both adsorbents, the adsorption amount of OTC increased significantly with a rise of the initial concentration. The adsorption data were severally fitted to Langmuir (Fig. 6C) and Freundlich (Fig. 6D) isotherms models to characterize the adsorption process and the thermodynamic parameters of the models were calculated (Table 4). The Langmuir model can better explain the isotherm adsorption behavior compared to the Freundlich model, as evidenced by a higher R^2 value. This suggests that the primary adsorption process involves monolayer chemisorption at specific active sites uniformly dispersed on the adsorbents' surface (Qin et al., 2021). Furthermore, the parameter $1/n$ was found to be less than 1, indicating favorable adsorption behavior and strong affinity towards OTC molecules for both MFM and CDs@MFM. CDs@MFM exhibited a lower $1/n$ value than MFM, implying a superior affinity for OTC due to the doped CDs on its surface. The maximum adsorption capacity (q_m) for OTC at 303 K was calculated to be 68.76 mg/g for MFM and 73.01 mg/g for CDs@MFM, highlighting the higher OTC uptake capacity of CDs@MFM. This enhancement is likely attributed to the modification of CDs, which provided adsorption sites with increased affinity and improved the material's specific surface area. Moreover, the adsorption capacity of CDs@MFM increased with temperature, suggesting an endothermic nature of OTC adsorption on MFM (Qi et al., 2023). Compared to other materials with a single adsorption function, CDs@MFM demonstrated competitive or superior adsorption capacity for OTC (Table 1). Although CDs@MFM had a relatively small adsorption capacity compared to some bifunctional materials owing to the limited specific surface area, it showed advantages in detection sensitivity, material cost, and simplicity of preparation, demonstrating its potential to detect and remove OTC residuals simultaneously from environmental water. Further studies to increase the specific surface area of CDs@MFM for ameliorating the OTC adsorption capacity were expected.

3.4. Mechanisms summary of superior detection and adsorption performance toward OTC by CDs@MFM

The proposed CDs@MFM material facilitated both the detection and adsorption processes of OTC, thus achieving higher detection sensitivity and adsorption capacity as anticipated. On one hand, the immobilized CDs could be quenched by OTC, likely through a combination of dynamic quenching and IFE mechanisms. Benefiting from the optimal specific surface area and pore structure of the composite, The adsorbed OTC on the surface of CDs@MFM resulted in a preconcentration effect, enhancing the interaction between OTC and the CDs within the framework, significantly improving the detection sensitivity than bare CDs. On the other hand, the incorporation of nanoscale CDs may increase the roughness of the material surface or creates interspaces between nanoparticles, thus providing more adsorption binding sites for OTC than bare MFM.

Table 2
Recovery studies of OTC in lake water samples by sensor.

Spiked (mg/L)	Detected (mg/L)	Recovery (%)	RSD (%) n = 3
0.10	0.115	115.0	2.68
	0.109	109.0	
	0.112	112.0	
2.00	2.032	101.6	5.25
	1.862	93.1	
	1.854	92.7	
6.00	5.734	95.6	1.63
	5.557	92.6	
	5.684	94.7	

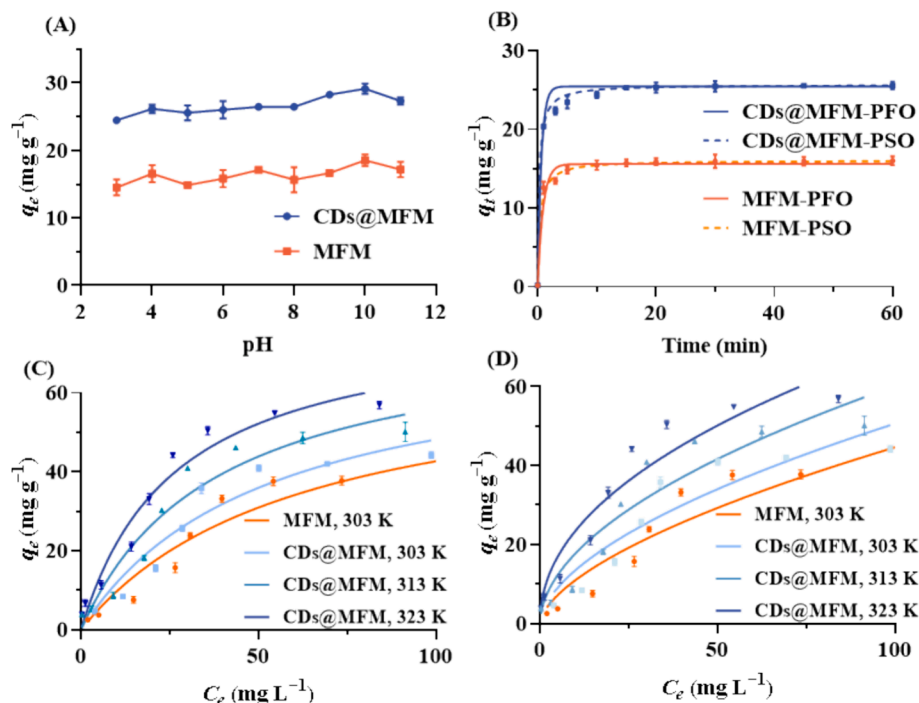


Fig. 6. Adsorption performance of OTC on CDs@MFM and MFM. (A) The adsorbed amount of OTC on CDs@MFM and MFM at different pH (3.0 ~ 11.0) with an initial OTC concentration of 50.0 mg/L. (B) The pseudo-first-order model and the pseudo-second-order model at an initial OTC concentration of 50.0 mg/L. Langmuir (C) and Freundlich (D) isotherm models of CDs@MFM for OTC adsorption under different temperatures (303 K, 313 K and 323 K).

Table 3

The adsorption kinetics parameters of MFM and CDs@MFM adsorption of OTC.

Adsorption kinetics	Parameters	MFM	CDs@MFM
Pseudo-first-order model	$q_{e,c}$ (mg/g)	15.60	25.46
	k_1 (min^{-1})	1.0951	1.6092
	R^2	0.9838	0.9925
Pseudo-second-order model	$q_{e,c}$ (mg/g)	16.08	25.68
	k_2 (g/mg min^{-1})	0.1497	0.1478
	R^2	0.9968	0.9984

Table 4

The parameters of Langmuir and Freundlich model of CDs@MFM for OTC adsorption at different temperatures.

	Langmuir Model			Freundlich Model		
	q_m (mg/g)	K_L (L/mg)	R^2	K_F (mg^{1+n} $\text{L}^{-1} \text{g}^{-1}$)	n	R^2
MFM, 303 K	68.76	0.0164	0.9221	2.7120	1.6443	0.8802
CDs@MFM, 303 K	73.01	0.0194	0.9191	3.6136	1.7445	0.8659
CDs@MFM, 313 K	77.14	0.0264	0.9378	5.2551	1.8896	0.8914
CDs@MFM, 323 K	79.82	0.0378	0.9629	7.9482	2.1236	0.9268

4. Conclusion

A novel dual-functional CDs@MFM material was developed for the simultaneous detection and removal of OTC, combining CDs as the fluorescent sensing unit with MFM as the substrate novelly. CDs@MFM retained the excellent fluorescence characteristics of CDs along with the structural properties of MFM, providing advantages in detection sensitivity, material cost, and ease of preparation. Due to the pre-enrichment effect of the porous structure, CDs@MFM showed higher sensitivity for OTC determination than bare CDs. Furthermore, the doped CDs on the

surface of CDs@MFM conferred a superior affinity for OTC, resulting in a slightly higher adsorption capacity than that of MFM. This suggests its potential for simultaneous detection and removal of OTC residues from environmental water. Future improvements could focus on optimizing the material preparation method and increasing the specific surface area to achieve better adsorption performance.

CRediT authorship contribution statement

Lu-Shuang Li: Writing – original draft, Funding acquisition, Conceptualization. **Su Li:** Methodology, Conceptualization. **Zong-Mei Huang:** Methodology. **Yan-Ting Song:** Software. **Wei Gong:** Project administration. **Jing Li:** Writing – review & editing, Funding acquisition, Conceptualization.

Declaration of competing interest

The authors declare that they have no known competing financial interests or personal relationships that could have appeared to influence the work reported in this paper.

Acknowledgments

The authors acknowledge the financial support of this research by the Natural Science Foundation of Hainan Province (No. 222RC547) and Hubei Province (No. 2022CFB964), the Starting Research Fund from the Hainan University (No. KYQD(ZR)19106) and the Research Fund from the Collaborative Innovation Center of One Health of Hainan University (XTCX2022JKB05).

References

- Alimohammadi, M., Sharifi, H., Tashkhourian, J., et al., 2023. An optical nose based on array of metal-doped carbon dots for identification of hazardous amines and assessing meat freshness. *Sens. Actuators B-Chem.* 393, 134274 <https://doi.org/10.1016/j.snb.2023.134274>.

- Bishwal, L., Kar, S., Bhattacharyya, S., 2023. Role of noncovalent interactions in N, P-functionalized luminescent carbon dots for ultrasensitive detection of moisture in D2O: Boosting visible-NIR light sensitivity. *ACS Appl. Mater. Interfaces*. 15, 15907–15916. <https://doi.org/10.1021/acami.3c01620>.
- Chang, Q., Ali, A., Su, J., et al., 2021. Simultaneous removal of nitrate, manganese, and tetracycline by *Zoogloea* sp. MFQ7: Adsorption mechanism of tetracycline by biological precipitation. *Bioresour. Technol.* 340, 125690 <https://doi.org/10.1016/j.biortech.2021.125690>.
- Chen, L.L., Xu, H., Wang, L., et al., 2020. Portable ratiometric probe based on the use of europium(III) coordination polymers doped with carbon dots for visual fluorometric determination of oxytetracycline. *Microchim. Acta*. 187, 125. <https://doi.org/10.1007/s00604-019-4104-3>.
- El-Malla, S.F., Elshenawy, E.A., Hammam, S.F., et al., 2022. Rapid microwave synthesis of N, S-doped carbon quantum dots as a novel turn off-on sensor for label-free determination of copper and etidronate disodium. *Anal. Chim. Acta*. 1197, 339491 <https://doi.org/10.1016/j.aca.2022.339491>.
- Fu, Y.Z., Huang, L., Zhao, S.J., et al., 2021. A carbon dot-based fluorometric probe for oxytetracycline detection utilizing a Förster resonance energy transfer mechanism. *Spectrosc. Acta Pt. A-Molec. Biomolec. Spectr.* 246, 118947 <https://doi.org/10.1016/j.saa.2020.118947>.
- Gai, S., Zhang, J., Fan, R.Q., et al., 2020. Highly stable zinc-based metal-organic frameworks and corresponding flexible composites for removal and detection of antibiotics in water. *ACS Appl. Mater. Interfaces*. 12, 28923. <https://doi.org/10.1021/acami.0c09495>.
- Guo, G., Li, T., Zheng, Q., et al., 2023. Dual-excitation carbon dots-based lateral flow visual sensing device for ratiometric determination and discrimination of tetracyclines in food. *Sens. Actuators B-Chem.* 395, 134523 <https://doi.org/10.1016/j.snb.2023.134523>.
- Hu, F., Fu, Q., Li, Y., et al., 2024. Zinc-doped carbon quantum dots-based ratiometric fluorescence probe for rapid, specific, and visual determination of tetracycline hydrochloride. *Food Chem.* 431, 137097 <https://doi.org/10.1016/j.foodchem.2023.137097>.
- Hu, T.W., Zeng, L.F., Li, Y.Q., et al., 2022. Multifunctional chitosan non-woven fabrics modified with terylene carbon dots for selective detection and efficient adsorption of Cr(VI). *Chem. Eng. J.* 432, 134202 <https://doi.org/10.1016/j.cej.2021.134202>.
- Li, J., Li, Q., Li, L.-S., et al., 2017. Removal of perfluorooctanoic acid from water with economical mesoporous melamine-formaldehyde resin microsphere. *Chem. Eng. J.* 320, 501–509. <https://doi.org/10.1016/j.cej.2017.03.073>.
- Li, L.S., Liang, H.W., Wu, C.T., et al., 2023b. A ratiometric fluorescence sensor for tetracycline detection based on two fluorophores derived from Partridge tea. *Microchim. Acta*. 190, 66. <https://doi.org/10.1007/s00604-023-05653-x>.
- Li, C., Liu, L., Zhang, D., 2024. Aggregation enhanced emissive orange carbon dots for information encryption and detection of Fe³⁺ and tetracycline. *Spectrochim. Acta. A Mol. Biomol. Spectrosc.* 305, 123504 <https://doi.org/10.1016/j.saa.2023.123504>.
- Li, Y., Wang, J., Huang, Z., et al., 2021. An Eu-doped Zr-metal-organic framework for simultaneous detection and removal of antibiotic tetracycline. *J. Environ. Chem. Eng.* 9, 106012 <https://doi.org/10.1016/j.jece.2021.106012>.
- Li, Y., Wang, Y., Du, P., et al., 2022. Fabrication of carbon dots@hierarchical mesoporous ZIF-8 for simultaneous ratiometric fluorescence detection and removal of tetracycline antibiotics. *Sens. Actuators B-Chem.* 358, 131526 <https://doi.org/10.1016/j.snb.2022.131526>.
- Li, L.-S., Xu, L., 2020. Highly fluorescent silicon quantum dots decorated silica microspheres for selective detection and removal of Au³⁺ and subsequent catalytic application. *J. Ind. Eng. Chem.* 84, 375–383. <https://doi.org/10.1016/j.jiec.2020.01.021>.
- Li, L.-S., Jiao, X.-Y., Zhang, Y., et al., 2018a. Green synthesis of fluorescent carbon dots from Hongcaitai for selective detection of hypochlorite and mercuric ions and cell imaging. *Sens. Actuators B-Chem.* 263, 426–435. <https://doi.org/10.1016/j.snb.2018.02.141>.
- Li, L.-S., Jiao, X.-Y., Zhang, Y., et al., 2018b. Highly fluorescent carbon dots synthesized with binary dopants for “turn off” and “turn off-on” sensing and cell imaging. *Sens. Actuators B-Chem.* 268, 84–92. <https://doi.org/10.1016/j.snb.2018.03.189>.
- Li, J., Yao, R.H., Deng, B.W., et al., 2023a. A facile construction of bifunctional core-shell structured magnetic metal-organic frameworks for detection and removal of tetracycline. *Chem. Eng. J.* 464, 142626 <https://doi.org/10.1016/j.cej.2023.142626>.
- Liu, Y.S., Guo, H., Wu, N., et al., 2023. Eu³⁺-Functionalized nanoporous covalent organic frameworks for fluorescence detection and removal of tetracycline. *ACS Appl. Nano Mater.* 6, 6627–6636. <https://doi.org/10.1021/acsnm.3c00323>.
- Liu, X.J., Li, H.Q., Lin, X.Y., et al., 2015. Synthesis of siloxane-modified melamine-formaldehyde microsphere and its heavy metal ions adsorption by coordination effects. *Colloids Surf. Physicochem. Eng. Aspects.* 482, 491–499. <https://doi.org/10.1016/j.colsurfa.2015.06.051>.
- Liu, Y., Su, X., Chen, L., et al., 2021. Green preparation of carbon dots from *Momordica charantia* L. for rapid and effective sensing of p-aminoazobenzene in environmental samples. *Environ. Res.* 198, 111279 <https://doi.org/10.1016/j.envres.2021.111279>.
- Liu, Y., Zhou, P., Wu, Y., et al., 2022. Fast and efficient “on-off-on” fluorescent sensor from N-doped carbon dots for detection of mercury and iodine ions in environmental water. *Sci. Total Environ.* 827, 154357 <https://doi.org/10.1016/j.scitotenv.2022.154357>.
- Liu, Y., Su, X., Liu, H., et al., 2025. Construction of eco-friendly dual carbon dots ratiometric fluorescence probe for highly selective and efficient sensing mercury ion. *J. Environ. Sci.* 148, 1–12. <https://doi.org/10.1016/j.jes.2024.01.013>.
- Lu, Y.F., Yu, L., Zhang, S.L., et al., 2023. Dual-functional fluorescent metal-organic framework based beads for visual detection and removal of oxytetracycline in real aqueous solution. *Appl. Surf. Sci.* 625, 157202 <https://doi.org/10.1016/j.apsusc.2023.157202>.
- Ming, G., Duan, H., Meng, X., et al., 2016. A novel fabrication of monodisperse melamine-formaldehyde resin microspheres to adsorb lead (II). *Chem. Eng. J.* 288, 745–757. <https://doi.org/10.1016/j.cej.2015.12.007>.
- Qi, X.M., Chen, Y.Z., Peng, J.W., et al., 2023. Non-cytotoxic fluorescent wood for selective detection and efficient removal of tetracycline. *Chem. Eng. J.* 466, 143284 <https://doi.org/10.1016/j.cej.2023.143284>.
- Qin, S., Yu, X., Xu, L., 2021. Amplified fluorescence detection and adsorption of Au³⁺ by the fluorescent melamine formaldehyde microspheres incorporated with N and S co-doped carbon dots. *J. Hazard. Mater.* 405, 123978 <https://doi.org/10.1016/j.jhazmat.2020.123978>.
- Rasheed, T., 2023. Carbon dots as robust class of sustainable and environment friendlier nano/optical sensors for pesticide recognition from wastewater. *Trends Anal. Chem.* 160, 116957 <https://doi.org/10.1016/j.trac.2023.116957>.
- Stacy, B.J., Nagasaki, K., Korgel, B.A., 2024. Luminescent Silicon Nanocrystals as Metal Ion Sensors. *ACS Nano*. 18, 15744–15753. <https://doi.org/10.1021/acsnano.4c02309>.
- Sun, S., Jiang, Q., Zhang, W., et al., 2022. Efficient adsorption of tetracycline in aquatic system by thermally-treated sediment. *Environ. Res.* 214, 113779 <https://doi.org/10.1016/j.envres.2022.113779>.
- Venugopalan, P., Vidya, N., 2023. Microwave-assisted green synthesis of carbon dots derived from wild lemon (*Citrus pennivesiculata*) leaves as a fluorescent probe for tetracycline sensing in water. *Spectrochim. Acta. A Mol. Biomol. Spectrosc.* 286, 122024 <https://doi.org/10.1016/j.saa.2022.122024>.
- Wang, B., Gu, C., Jiao, Y., et al., 2023. Novel preparation of red fluorescent carbon dots for tetracycline sensing and its application in trace determination. *Talanta*. 253, 123975 <https://doi.org/10.1016/j.talanta.2022.123975>.
- Wang, Y.L., Ni, P.J., Jiang, S., et al., 2018. Highly sensitive fluorometric determination of oxytetracycline based on carbon dots and Fe₃O₄ MNPs. *Sens. Actuators B-Chem.* 254, 1118–1124. <https://doi.org/10.1016/j.snb.2017.07.182>.
- Wang, C., Sun, Q., Yang, M., et al., 2022. Preparation of highly luminescent nitrogen-doped carbon quantum dots and their detection of tetracycline antibiotics. *Colloids Surf. Physicochem. Eng. Aspects.* 653, 129982 <https://doi.org/10.1016/j.colsurfa.2022.129982>.
- Wang, W.J., Xu, Y.Q., Liu, X.Q., et al., 2020. Efficient fabrication of ratiometric fluorescence imprinting sensors based on organic-inorganic composite materials and highly sensitive detection of oxytetracycline in milk. *Microchem. J.* 157, 105053 <https://doi.org/10.1016/j.microc.2020.105053>.
- Wu, J., Chen, X., Zhang, Z., et al., 2022a. “Off-on” fluorescence probe based on green emissive carbon dots for the determination of Cu²⁺ ions and glyphosate and development of a smart sensing film for vegetable packaging. *Microchim. Acta*. 189, 131. <https://doi.org/10.1007/s00604-022-05241-5>.
- Wu, N., Guo, H., Wang, M., et al., 2022b. A novel core-shell coordination assembled hybrid via postsynthetic metal exchange for simultaneous detection and removal of tetracycline. *Anal. Chim. Acta*. 1190, 339247 <https://doi.org/10.1016/j.aca.2021.339247>.
- Yang, Q.F., Hong, H., Luo, Y.K., 2020. Heterogeneous nucleation and synthesis of carbon dots hybrid Zr-based MOFs for simultaneous recognition and effective removal of tetracycline. *Chem. Eng. J.* 392, 123680 <https://doi.org/10.1016/j.cej.2019.123680>.
- Zhang, X., Lin, X., He, Y., et al., 2019. Study on adsorption of tetracycline by Cu-immobilized alginate adsorbent from water environment. *Int. J. Biol. Macromol.* 124, 418–428. <https://doi.org/10.1016/j.ijbiomac.2018.11.218>.
- Zhang, L., Wang, J., Wang, H.T., et al., 2021. Rational design of smart adsorbent equipped with a sensitive indicator via ligand exchange: A hierarchical porous mixed-ligand MOF for simultaneous removal and detection of Hg²⁺. *Nano Res.* 14, 1523–1532. <https://doi.org/10.1007/s12274-020-3211-0>.
- Zhao, Y.J., Wang, Q.Z., Wang, H.H., et al., 2021. Europium-based metal-organic framework containing characteristic metal chains: A novel turn-on fluorescence sensor for simultaneous high-performance detection and removal of tetracycline. *Sens. Actuators B-Chem.* 334, 129610 <https://doi.org/10.1016/j.snb.2021.129610>.
- Zhou, Y., Yang, Q., Zhang, D.N., et al., 2018. Detection and removal of antibiotic tetracycline in water with a highly stable luminescent MOF. *Sens. Actuators B-Chem.* 262, 137–143. <https://doi.org/10.1016/j.snb.2018.01.218>.
- Zhu, T., Cao, L., Kou, X., et al., 2022. Nitrogen-doped cyan-emissive carbon quantum dots for fluorescence tetracycline detection and lysosome imaging. *RSC Adv.* 12, 33761–33771. <https://doi.org/10.1039/d2ra04945g>.
- Zu, F., Yan, F., Bai, Z., et al., 2017. The quenching of the fluorescence of carbon dots: A review on mechanisms and applications. *Microchim. Acta*. 184, 1899–1914. <https://doi.org/10.1007/s00604-017-2318-9>.